Available online at www.sciencedirect.com
ScienceDirect
Progress in Oceanography 75 (2007) 348–362
Progress in Oceanography
www.elsevier.com/locate/pocean

Near-inertial motions over the continental shelf off Concepción, central Chile

Marcus Sobarzo [a,*], R. Kipp Shearman [b], Steve Lentz [c]

[a] Departamento de Oceanografía, Universidad de Concepción, Barrio Universitario s/n, Concepción, Chile
[b] College of Oceanic and Atmospheric Sciences, Oregon State University, 104 COAS Admin Bldg, Corvallis, OR 97331-5503, USA
[c] Department of Oceanography, Woods Hole Oceanographic Institution, Woods Hole, MA 02543, USA

Available online 2 September 2007

Abstract

The inertial response to wind forcing is studied on a continental shelf limited by two submarine canyons and near one of the biologically most important coastal areas in the Chile–Peru upwelling system (35°57′S–37°15′S). After a brief description of the tides (M_2 and K_1), the paper focuses on the temporal and spatial variability of the near-inertial band (0.045–0.055 cph), which accounts for 2.6–61.5% of the total observed current variance. Common features of near-inertial motion, especially the 180° phase difference between the upper and the lowers layers and the intermittency of this motion, are described for the first time for the Chilean shelf. Outstanding aspects appear when comparing the near-inertial currents in the inner shelf with those near the shelf break, where the subinertial background flow changes the effective Coriolis frequency, generating resonance between the near-inertial currents and the daily wind cycle. Also, the amplitudes of the near-inertial currents were stronger near the shelf break (about 20 cm s^{-1}) and weaker near the coast (about 5 cm s^{-1}). Intermittency in the enhanced near-inertial motions varied around 3.5–10 days and appears to be related to the beat period between diurnal and near-inertial frequencies.

Keywords: Inertial motion; Sea breeze process; Coastal upwelling areas; Continental shelf; Effective Coriolis frequency; Central Chile

1. Introduction

Significant near-inertial oscillations (NIOs) in currents were observed from a moored array on the continental shelf off Concepción, Chile (36°30′S) in March 1994 (late austral summer). The observed near-inertial fluctuations accounted for a substantial amount (up to 62%) of the total observed current variance. The amplitudes of the near-inertial currents were stronger near the shelf break (about 20 cm s^{-1}) and weaker near the coast (about 5 cm s^{-1}). Typical features of NIOs were similar to those observed on other continental shelves (e.g., Millot and Crépon, 1981; Tintoré et al., 1995; Federiuk and Allen, 1996; Chen et al., 1996; Shearman, 2005) and include: anticyclonically-rotating circularly-polarized currents; an approximately 180° phase

* Corresponding author. Tel.: +56 41 220 4016; fax: +56 41 220 7076.
E-mail addresses: msobarz@udec.cl (M. Sobarzo), shearman@coas.oregonstate.edu (R.K. Shearman), slentz@whoi.edu (S. Lentz).

0079-6611/$ - see front matter
doi:10.1016/j.pocean.2007.08.021

difference between the upper and lower layers; temporal intermittency; and changes in the peak frequency due to shifts in the "effective" Coriolis frequency (Kunze, 1985) caused by horizontal shear in the subinertial flow near the shelf break.

The relationship between near-inertial oscillations and diurnal winds has received increasing attention (Lerczak et al., 2001; Hyder et al., 2002; Rippeth et al., 2002). Analytical models suggest that diurnal winds should drive currents whose amplitude will be particularly energetic close to 30° latitude, where diurnal and inertial periods are similar (Hyder et al., 2002).

Section 2 of this paper describes the observations and data analysis, including a brief description of tidal and subinertial currents; Section 3.1 discusses meteorological variability; Sections 3.2 and 3.3 highlight the principal features of the NIOs (vertical structure, horizontal structure, temporal variability); and Section 4 is a discussion of the effective Coriolis frequency and resonant forcing and inertial–diurnal beating.

2. Observations and data analysis

The study region over the continental shelf off Concepción, Chile, is bounded by the Itata Canyon to the north and the Biobío Canyon to the south. The continental shelf narrows from 60 km in the north to 25 km in the south over an alongshore expanse of 70 km (Sobarzo and Djurfeldt, 2004). On this shelf, there are several embayments, two important rivers (Biobío and Itata), and one prominent point (Punta Lavapié) that is moreover an important coastal upwelling site in southern Chile (Fig. 1).

Currents and hydrographic data were obtained from the Thioploca–Chile expedition carried out during late summer (March, April) 1994. Eighteen sensor-data current meters with sampling periods of 10 or 30 min were suspended on six moorings (three current meters on each mooring in the upper, middle, and lower parts of the water column). The mooring sites are named according to their relative positions on the shelf (North-Ocean, North-Coast, Central-Ocean, Central-Coast, South-Ocean, South-Coast). Accuracy values, provided by the meter manufacturer, are: ± 0.5 cm s^{-1} (velocity), $\pm 2°$ (direction resolution), and ± 0.1 °C (temperature). An along-coast Cartesian coordinate system (x:u, y:v, z:w) was used with y:v positive toward 18° with respect to true north. Meteorological variables (wind speed and direction, air surface temperature, radiation) were measured at Punta Hualpén (Fig. 1) using a DELTA-T station (model DL) with a sampling interval of 10 min and an accuracy of $\pm 2°$ (direction, winds over 5 m s^{-1}) and 0.1 m s^{-1} (magnitude). Hourly data sets were formed by block averaging the raw data.

Near-inertial motion was studied after removing the tidal current predictions from an harmonic analysis and removing subinertial variability by subtracting low-pass-filtered time series (the symmetric filter has a half power at 0.6 cpd and spans 121 h). A wavelet analysis, using a Morlet wavelet with a width of six periods, was applied to identify the intrinsic frequency of near-inertial variability (Shearman, 2005).

2.1. Tidal variability

Tidal amplitudes and phases were estimated by means of harmonic analysis (Pawlowicz et al., 2002). Phases are reported in degrees (°G) relative to the maximum of the tidal potential at Greenwich for each constituent. Uncertainties (95% confidence intervals) in the amplitudes and phases from the harmonic analysis were estimated according to Pawlowicz et al. (2002). Only the M_2 and K_1 constituents are reported because the time series are too short to accurately estimate the other constituents.

Tidal currents are relatively weak, accounting for 18% or less of the total current variance. The M_2 major axis amplitudes are less than 3 cm s^{-1} and strongest at the Center-Ocean and South-Ocean moorings (Fig. 2). The M_2 tidal ellipses are strongly polarized and, near the coast, oriented along-shelf; over the outer shelf, they are variable. The K_1 major axes showed surfaces amplitudes between 7.1 and 2.3 cm s^{-1} near the shelf break and less than 2.5 cm s^{-1} near the coast (not shown). In most cases, this constituent was uncertain.

2.2. Subinertial variability

Sobarzo and Djurfeldt (2004) showed that the first empirical mode of the subinertial current observations (45% of the subinertial variance) corresponds to an along-shore flow responding to the intensification of

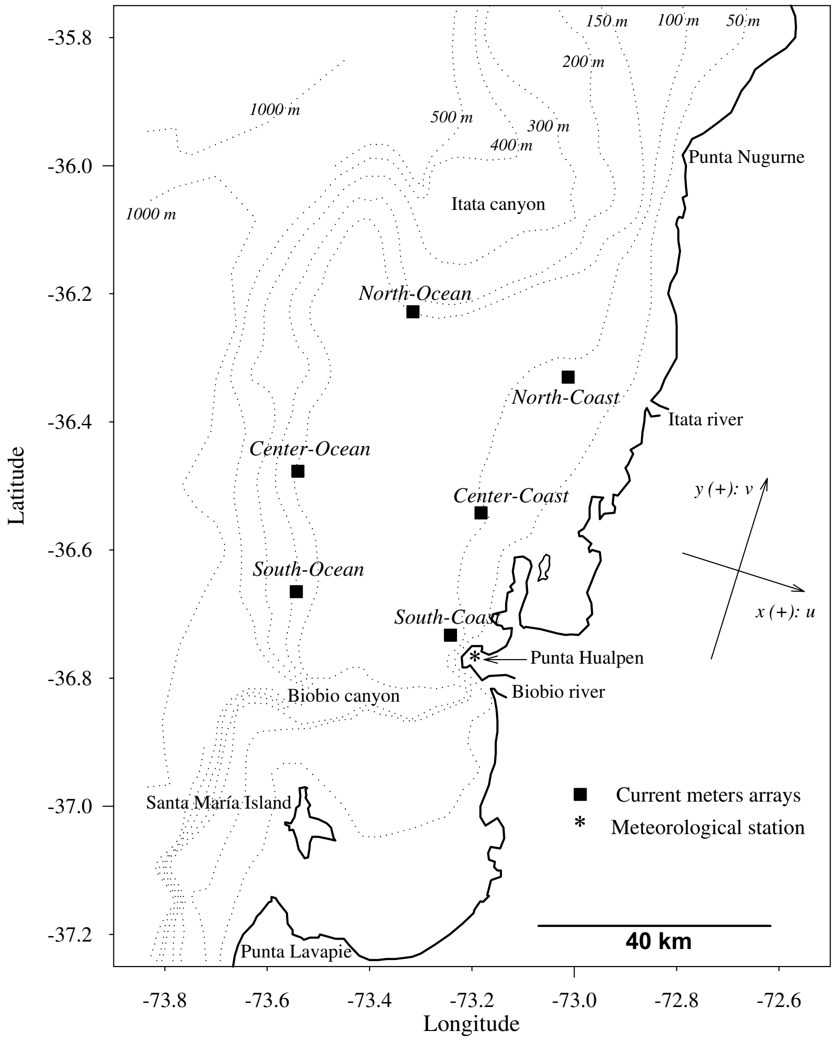

Fig. 1. Study area showing the locations of the moorings and the meteorological station. Thioploca Cruise, March 1994.

south-westerly winds on a 3–10 day scale. The second mode is dominated by the cross-shore fluctuations at the shelf break. Ekman transport based on the wind stress and the observed transport in the surface boundary layer are highly correlated over the north and central shelf. Near the bottom, a mean southward flow was found with a clear southward intensification induced by the bathymetry and probably by a meridional pressure gradient.

3. Results

3.1. Meteorological setting – diurnal wind variability

Winds measured at Punta Hualpén have a major principal axis explaining 95.2% of the total variance oriented primarily along-shore toward 38° with respect to geographical north; the mean wind is oriented toward the north-east at 2.8 m s^{-1} (Fig. 3f). The rotary spectra from 7 March to 5 April 1994 have a significant peak (with 8 degrees of freedom) near the diurnal period with slightly more anticlockwise energy than clockwise energy, consistent with a sea breeze (Simpson, 1995) (Fig. 3g). The square of the ratio of the minor (1.1 m s^{-1}) to major (2.7 m s^{-1}) ellipse axes (ε^{-2}) was 0.16 for the diurnal winds (high-passed, periods less than 40 h).

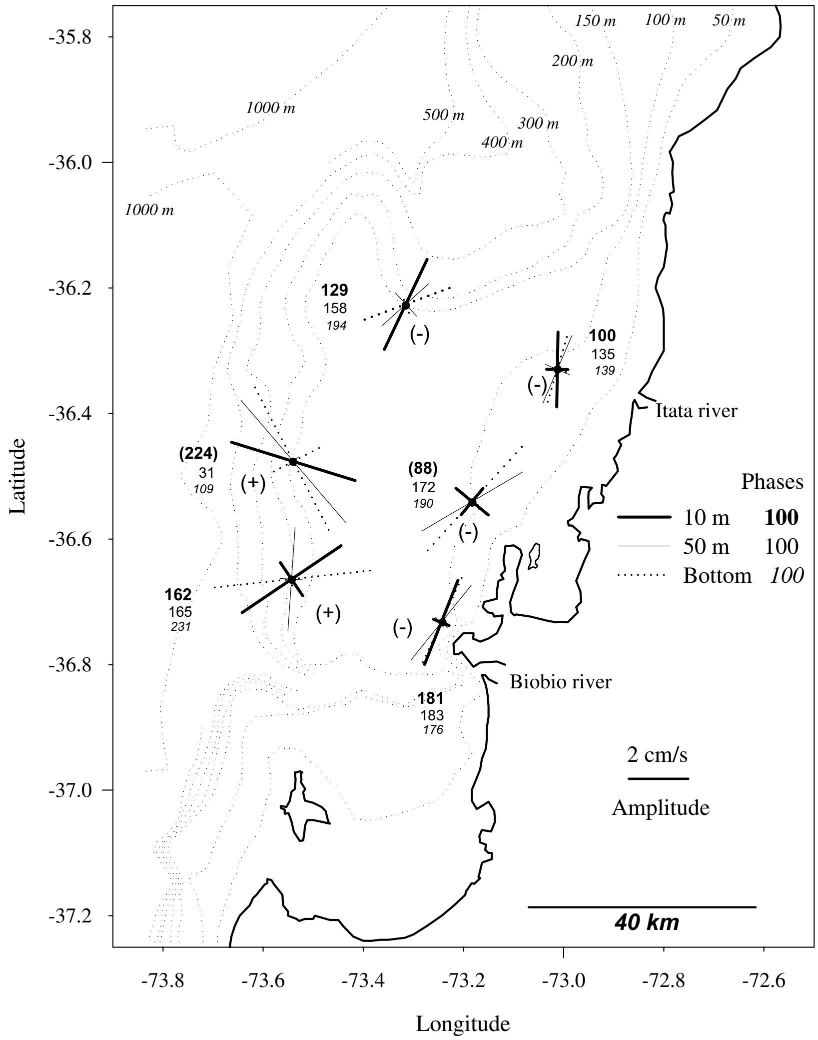

Fig. 2. Tidal current major and minor axes, orientation, and phases for $M2$ at 10 m, 50 m, and bottom depths. Phases in parentheses are not significant at the 95% confidence level. (+) indicates anticlockwise rotation and (−) clockwise rotation of M_2 tidal currents.

The strength of the sea breeze depends on the synoptic scale meteorological conditions. With winds from the south-west (anticyclonic circulation) (positive winds Fig. 3b), the daily cycles of solar radiation (amplitudes of about 900 W m^{-2}) and air surface temperature (AST; >5 °C) are strongest (Fig. 3b,e). During these clear and warm conditions, the high-passed (< 40 h) time series of cross-shore and along-shore winds show a clear and relatively strong daily cycle (Fig. 3c,d).

When the winds reverse and blow from the north-east (cyclonic circulation; 17–19 March; 22–23 March; 30 March-2 April), cloudiness increases, the daily cycles of solar radiation and AST diminish, and the sea breeze disappears (Fig. 3b–e).

The intense diurnal variability of wind, AST, and solar radiation during anticyclonic wind circulation has a very clear response in the sea surface temperature at 10 m depth. This is observed in the correlation between the first empirical orthogonal function of temperatures (73%) coming from current meters at 10 m depth from North-Coast, South-Ocean, Center-Ocean, and North-Ocean moorings and the AST ($r = 0.7$, Fig. 3e). This EOF is also highly correlated with solar radiation and winds.

The alternation between anticyclonic and cyclonic wind circulation is linked to the poleward propagation of atmospheric low-pressure systems (Shaffer et al., 1997; Hill et al., 1998). In Chile, the influence of these low-

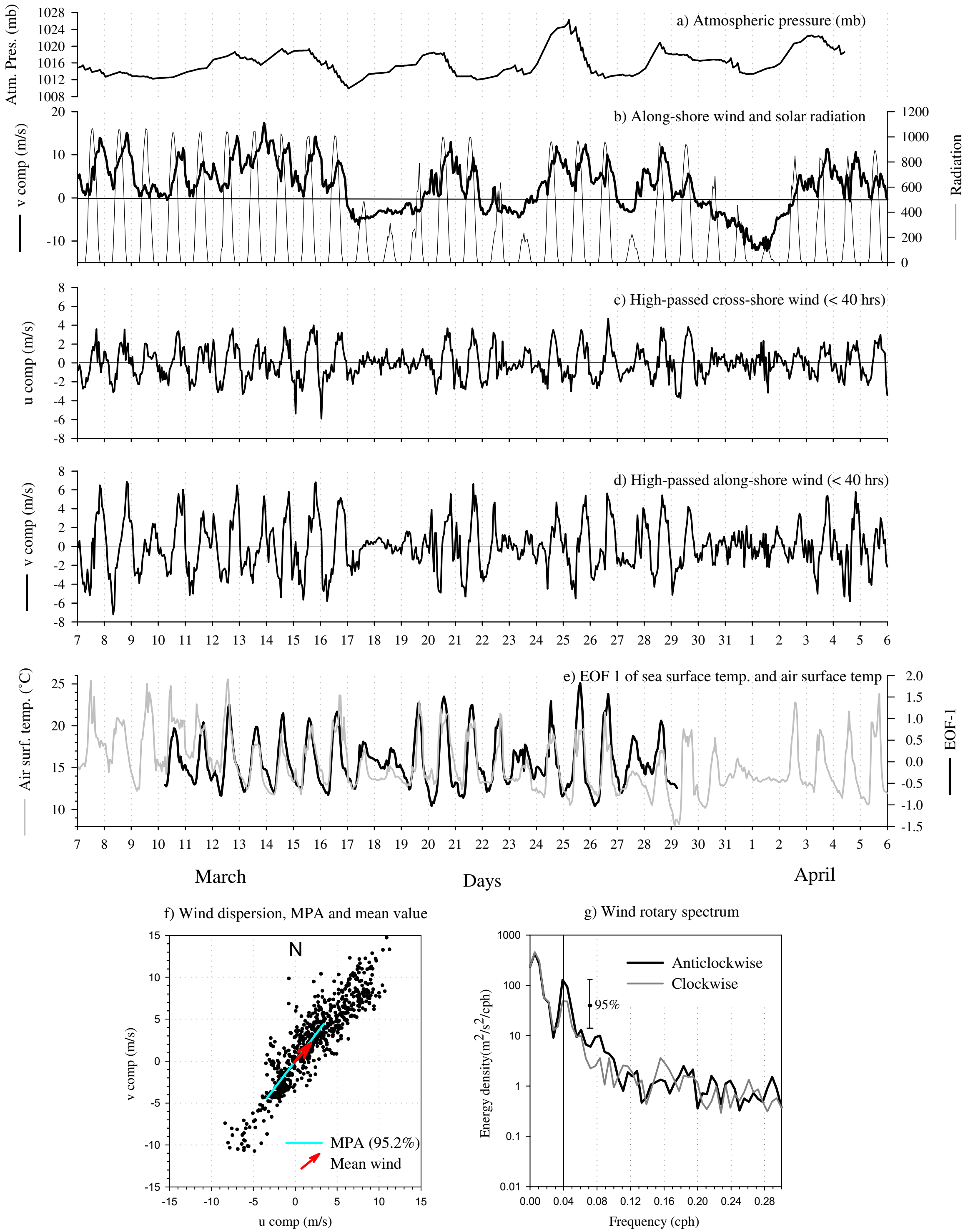

Fig. 3. Diurnal variability of (a) atmospheric pressure, (b) alongshore wind and solar radiation, (c) high-passed cross-shore, and (d) alongshore wind; and (e) air surface temperature and first EOF of sea surface temperature. A scatter plot of wind components showing (f) orientation of winds and (g) rotary spectra of wind.

pressure systems extends from about 20–40°S (Rutllant and Garreaud, 1995) and is associated with variations in cloudiness and solar radiation with periods of 3–10 days. During our study, wind, radiation, and air surface temperature respond to this poleward propagation with fluctuations between 4 and 5 days resulting in a sea breeze with this same temporal variability (Fig. 3c,d).

3.2. Magnitude and relative intensity of NIOs

The notable diurnal variation in the summer meteorological conditions of this coastal environment is near the inertial frequency, $f = 0.0496$ cph (or 1/20.13 cph). All the current time series show some near-inertial peaks in the anticlockwise component of the rotary spectra that are much larger than the clockwise component, consistent with inertial oscillations (e.g., North-Coast 10 m, Fig. 4a,b). Here, rotary spectra were calculated using hourly raw data from each current meter and applying a Hanning window before calculating the spectra. To maximize the frequency resolution, the spectra were not ensemble-averaged in time (Lerczak et al., 2001). Table 1 shows comparisons, for each current meter, of the percentage of the total variance in each of the following frequency bands: (1) Diurnal (K_1–O_1: 1/26–1/22 cph); (2) Near-inertial (1/22–1/16 cph); (3) Semidiurnal (M_2–S_2: 1/14–1/10 cph); and (4) Subinertial (1/216–1/72 cph). Roughly one third or more of the current variance is in the near-inertial band at most of the current meter sites. The lowest percentage of spectral density in the near-inertial band is found at the South-Coast mooring and the highest percentages are located at 10 m depth at the Center-Coast, North-Coast, and North-Ocean moorings. Subinertial variability is more intense at the Center-Ocean (10 m depth), North-Coast (70 m depth), Center-Coast (70 m depth), and South-Coast moorings.

The along-shore and cross-shore current components were detided and high passed (<40 h) to isolate near-inertial variability. In most cases, near-inertial u and v have similar magnitudes and u leads v by 90°, as expected for anticlockwise circular near-inertial currents. Also, near-inertial currents at 10 m and near the bottom are approximately 180° out of phase (Fig. 5), as observed over other continental shelves (e.g., Millot and Crépon, 1981; Salat et al., 1992; Rippeth et al., 2002).

3.3. Temporal variations and the intermittency of NIOs

NIOs are intermittent on time scales of a few days with amplitudes of 10–20 cm s^{-1} during strong events (Fig. 5,6). The temporal variation and intermittency of NIOs are highlighted in time–frequency representations using wavelet analysis on the along-shore flow (Fig. 6). The cross-shore component is similar and is not shown. The largest NIOs are observed near the shelf break at the Center-Ocean and South-Ocean moorings. Along the outer shelf, the bursts of surface inertial energy are spatially coherent and related to the wind diurnal energy (Fig. 6f,g,h). Inner shelf bursts of inertial energy appear every 3–4 days at the North-Coast mooring (Fig. 6a) and are irregular at the Center-Coast mooring (Fig. 6b). At the South-Coast mooring, closer to shore, near-inertial variability is nearly absent (Figs. 6c, 5). This inner-shelf variability does not appear to be related to the wind diurnal energy (Fig. 6d) or the outer-shelf bursts. The cross-shelf decrease in near-inertial energy, notably at the South-Coast site, suggests the influence of the coastal boundary condition or friction (e.g., Shearman, 2005).

The complete structure on the shelf of the detided and high-passed time series was analyzed using empirical orthogonal functions. Here, we use a 7-day common time period of onshore and along-shore components from each current meter (36 time series) as if they were scalar time series. The amplitudes of the first and second "overall" EOFs (31% and 20% of the total variance, respectively) are shown in Fig. 7b in relation to mechanical wind energy (wind^3). Wind time series show the intensification of the south-westerlies from 12–14 March (upwelling event, Fig. 7a). The amplitudes of EOFs 1 and 2 exhibit near-inertial oscillations that decrease during this event and increase after it.

In separate EOF analyzes of the currents along the shelf break and near the coast, the energy of the first two EOFs in each case increased relative to the overall EOF. Near the coast, EOF 1 accounted for 39% of the variance and EOF 2 for 24%. Along the shelf break, EOF 1 accounted for 35% of the variance and EOF 2 for 21%. The amplitude of these modes is given in Figs. 7c and d. The amplitude is more intense along the outer shelf, decreasing during the upwelling event and showing a strong intensification after this event.

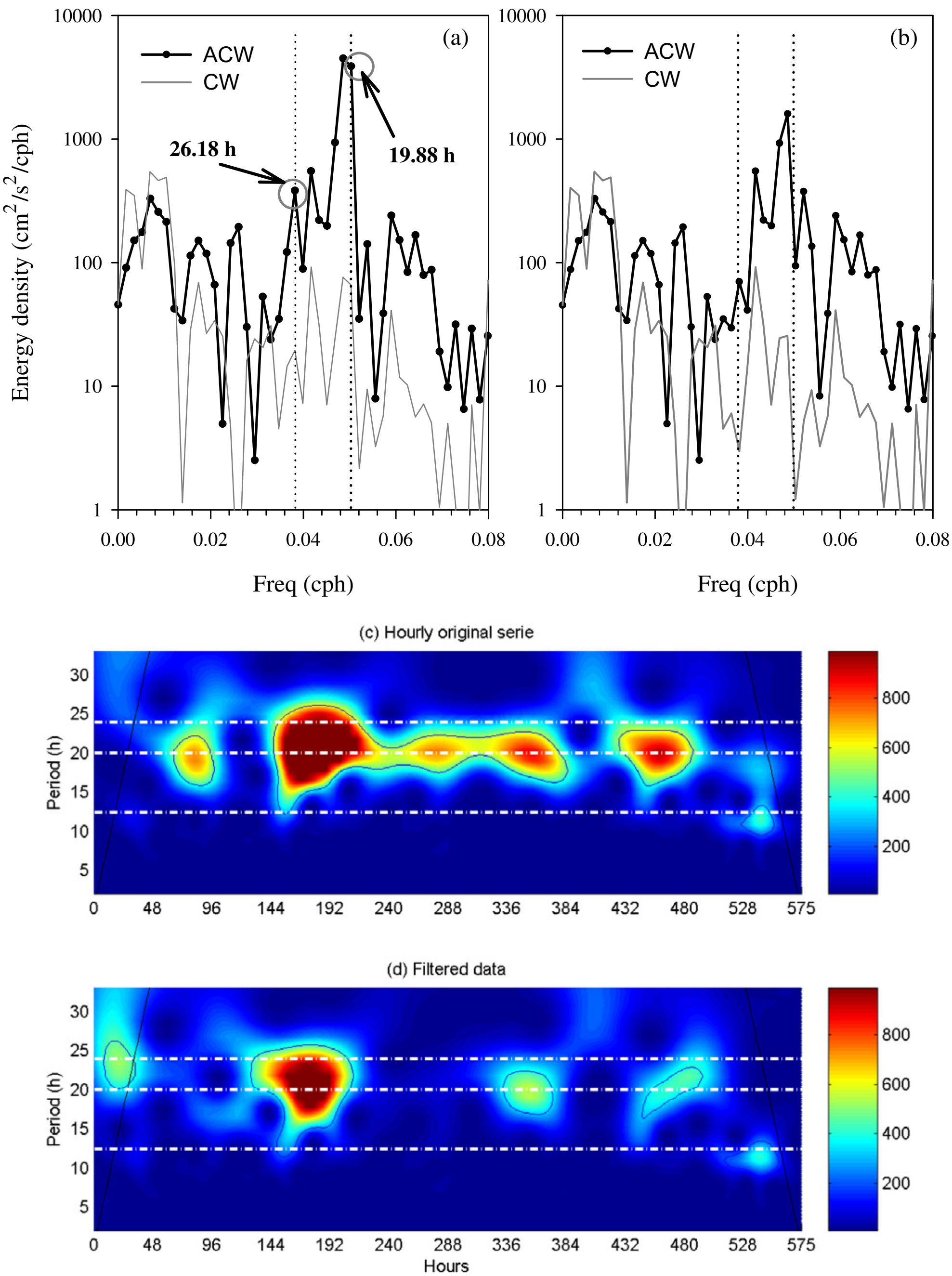

Fig. 4. Rotary spectra from North-Coast mooring at 10 m depth. (a) Hourly raw series, (b) series without 19.88 h and 26.18 h, (c) wavelet of original series, (d) wavelet of filtered data. In (a) and (b), the vertical lines mark harmonics that were extracted. Color scale in cm^2/s^2.

Extending the time series until 28 March by leaving out the short current time series at 50 m depth (Center-Coast, Center-Ocean) and at 10 and 110 m depth (South-Ocean), other near-inertial energy intensification events related to south-westerly wind intensifications on 20–21 March and 24–26 March are evident (Fig. 7e).

Table 1
A comparison between the major axes of the M_2 and near-inertial currents, and the percentage of total variance in the semidiurnal, diurnal, inertial, and subinertial frequency bands for each current meter deployed on the continental shelf off Concepción

Moorings	Depths (m)	Major axis (cm s^{-1})		Percentage of spectral density (%)			
		M_2	Inertial current	Semidiurnal	Diurnal	Near inertial	Subinertial
South-Coast	10	1.5 ± 0.8	2.5	9.9	1.8	10.9	33.3
	50	1.6 ± 0.4	2.1	5.6	3.0	9.5	57.8
	70	1.7 ± 0.5	1.9	4.5	1.5	3.8	68.8
South-Ocean	10	2.0 ± 1.3	9.9	8.2	23.4	21.2	8.1
	50	1.8 ± 0.7	5.8	4.7	26.6	36.7	4.2
	110	2.7 ± 1.1	5.5	14.5	1.0	42.3	5.5
Center-Coast	10	0.7 ± 0.7	5.3	5.2	3.0	64.6	8.3
	50	2.0 ± 0.7	3.0	15.2	8.3	16.7	8.5
	70	2.5 ± 0.5	3.0	14.8	3.4	33.6	17.1
Center-Ocean	10	2.2 ± 2.0	9.0	5.9	9.7	9.7	28.5
	50	2.7 ± 1.0	6.6	7.8	12.0	42.7	6.3
	120	2.8 ± 0.6	5.0	9.4	9.2	44.9	12.2
North-Coast	10	1.3 ± 0.5	5.3	2.3	5.7	53.2	14.1
	50	1.3 ± 0.3	1.7	10.4	9.4	29.7	11.5
	70	1.1 ± 0.3	1.3	9.6	7.5	31.9	23.3
North-Ocean	10	1.7 ± 0.7	6.2	2.9	4.9	67.9	6.4
	50	1.1 ± 0.4	2.7	3.5	6.2	38.0	13.1
	80	1.6 ± 0.9	3.9	7.6	6.7	47.8	15.1
Average		*1.8 ± 0.7*	*4.5*	*7.9*	*8.0*	*33.6*	*19.0*

4. Discussion

The near-inertial current variability shows distinctively different features between the coast and the ocean moorings. Here, we explore the physical processes behind these differences.

4.1. Offshore near-inertial current variability: effective Coriolis frequency and resonant forcing

At the Center-Ocean and South-Ocean moorings, there is a shift in the peak inertial energy toward lower frequencies in contrast to the other sites (compare Figs. 6g,h with a,b,c,f). Kunze (1985) and Shearman (2005), among others, observed a similar shift to lower frequencies caused by a mean (or persistent with respect to the near-inertial variability) lateral current shear. They estimated an effective Coriolis (inertial) frequency (f_{eff}) given by:

$$f_{\text{eff}} = f + \frac{\zeta}{2} \tag{1}$$

where ζ is the vertical component of the relative vorticity of the subinertial currents. Hence, the frequency shift is $\zeta/2$. To determine whether this is the cause for the shift in inertial energy toward lower frequencies at the Center-Ocean and South-Ocean moorings, the relative vorticity of the subinertial flow is estimated.

The relative vorticity (ζ) can be estimated by:

$$\frac{\partial v}{\partial x} = \frac{v_{\text{Southcoast}} - v_{\text{Southocean}}}{23\ \text{km}} \tag{2}$$

$$\frac{\partial u}{\partial y} = \frac{u_{\text{Centerocean}} - u_{\text{Southocean}}}{22\ km} \tag{3}$$

$$\zeta = \frac{\partial v}{\partial x} - \frac{\partial u}{\partial y} \tag{4}$$

using the 10 m depth subinertial current records from the South-Ocean, Center-Ocean, and South-Coast sites (Fig. 1). The relative vorticity due to ($\partial v/\partial x$) and $-(\partial u/\partial y)$ estimated from the low-passed currents ranges from $0.1\,f$ to $-0.2\,f$, and shows a clockwise tendency (negative vorticity, cyclonic) in the case of the ($\partial v/\partial x$) (heavy

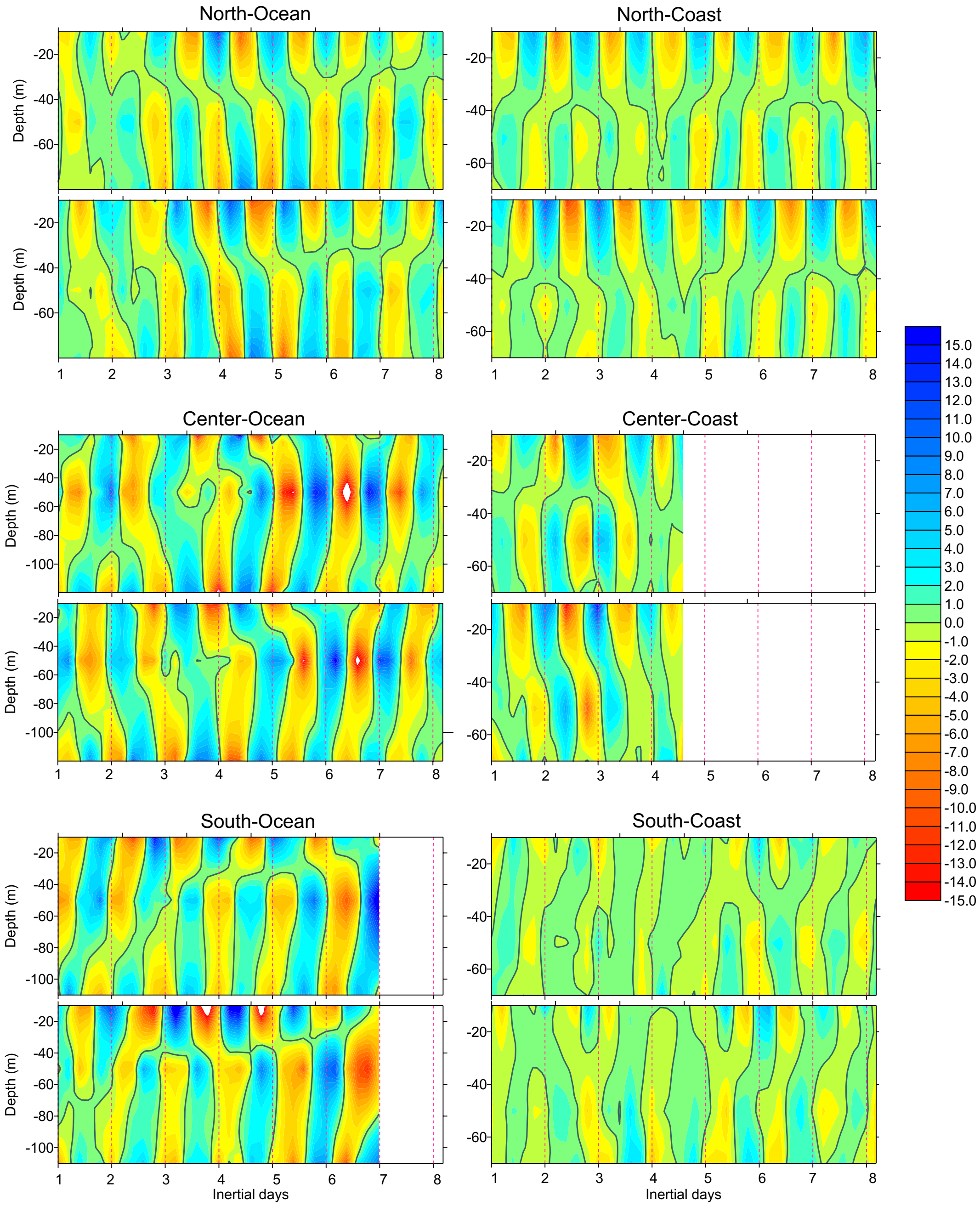

Fig. 5. Cross-shore (upper) and along-shore (below) currents for each mooring as a function of depth and time for the period March 14–19. Time series have been detided and high-pass filtered to isolate near-inertial motions (period near 20 h). Color scale is cm s^{-1}.

line shows South-Coast–South-Ocean, Fig. 8a) and anticlockwise tendency (positive vorticity, anticyclonic) in the case of the $-(\partial u/\partial y)$ (heavy line shows Center-Ocean–South-Ocean, Fig. 8b). For purposes of comparison, we also included surface vorticity estimates from all the moorings (10 m depth) in these figures. The effective Coriolis frequency calculated using $(f+\zeta/2)$ gives inertial estimates near to the peak wavelet period with a mean value about 3% greater than in the inertial period (Fig. 8c). This result is only suggestive, since the effective Coriolis frequency was calculated using $\zeta = -(\partial u/\partial y)$ because the moored array does not completely

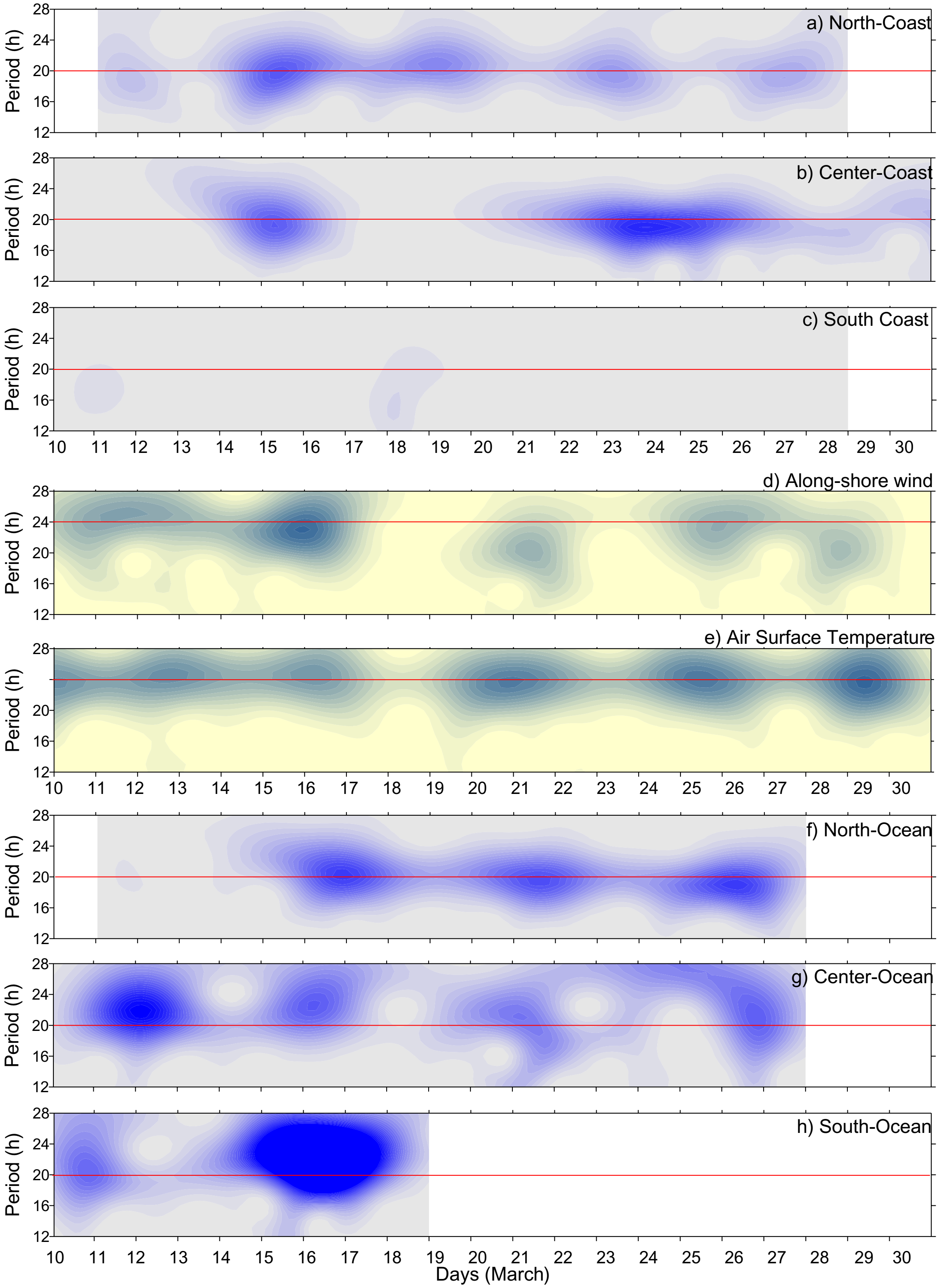

Fig. 6. Wavelet power spectrum for the near-surface along-shore component of the detided and high-pass-filtered current time series at each mooring site (a–c, f–h). Along-shore wind (d) and air surface temperature (e) are included.

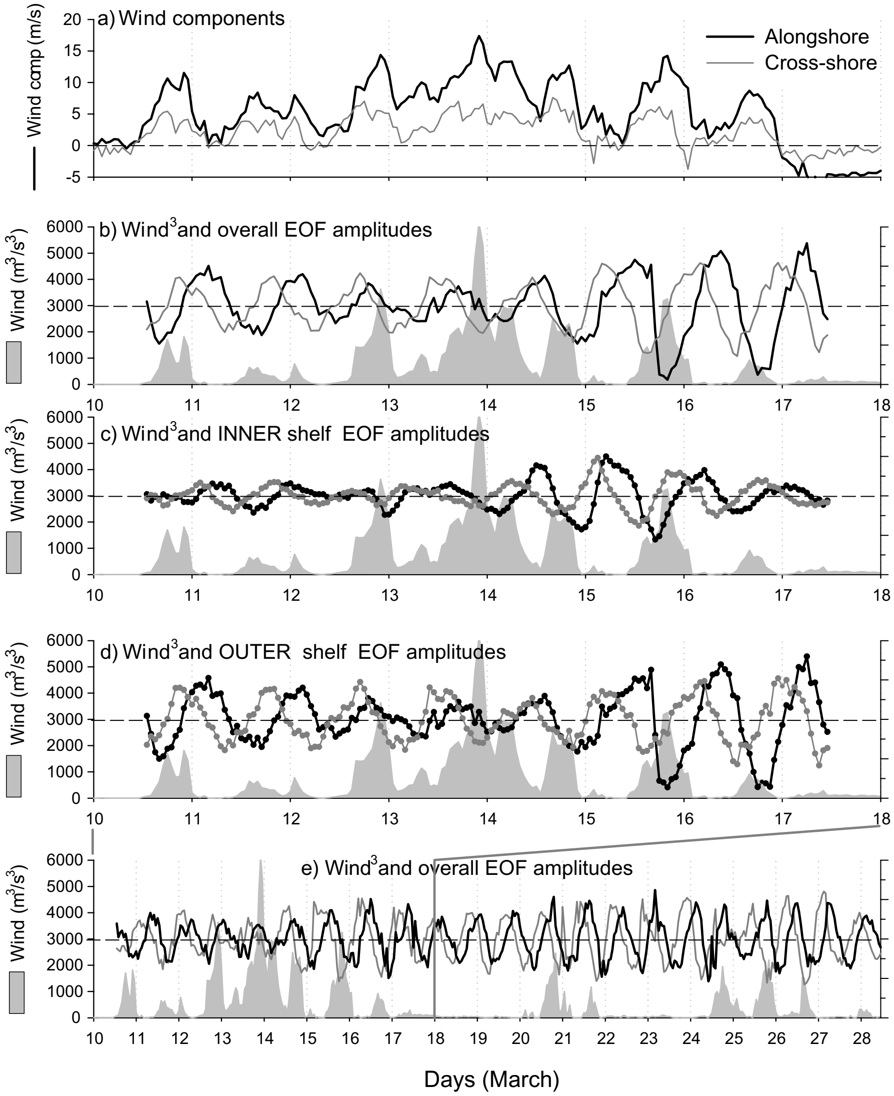

Fig. 7. (a) Along-shore and cross-shore wind components; (b) Wind^3 and overall EOF amplitudes; (c) Wind^3 and inner-shelf EOF amplitudes; (d) Wind^3 and outer-shelf EOF amplitudes; (e) same as b but using a longer time series. EOF-1: black line. EOF-2: gray line.

resolve the relevant spatial scales; and we believe the estimate of $(\partial v/\partial x)$ is centered too far inshore, whereas -$(\partial u/\partial y)$ is more correctly co-located and representative of the offshore moorings. The cyclonic vorticity exhibited by $(\partial v/\partial x)$ may play a role in isolating the inertial response at the coastal moorings. On the other hand, when we use both components to compute relative vorticity, we get anticyclonic vorticity, about half the amplitude of $-(\partial u/\partial y)/f$ alone.

Following Sobarzo and Djurfeldt (2004), the major principal axes and mean values of low-frequency currents ($\sigma < 0.025\ \mathrm{h}^{-1}$) at the South-Ocean and Center-Ocean moorings show an approximately anticyclonic flow with mean values of $4.8\ \mathrm{cm\ s}^{-1}$ and $-9.7\ \mathrm{cm\ s}^{-1}$, respectively. This anticyclonic tendency is due to a strong cross-isobath current shear at 10 m depth between the South-Ocean and Center-Ocean moorings (Fig. 9a), probably associated with an anticyclonic transport of cold water coming from Punta Lavapié (for instance, Fig. 9b). The mean relative vorticity $-(\partial u/\partial y)$ is anticyclonic, approximately $0.08\ |f|$.

Offshore near-inertial variability appears after upwelling-favorable wind events. During these upwelling events, diurnal wind is enhanced and the subtidal current response creates anticyclonic relative vorticity that shifts the effective Coriolis frequency lower, towards the diurnal frequency. Like the Lerczak et al. (2001)

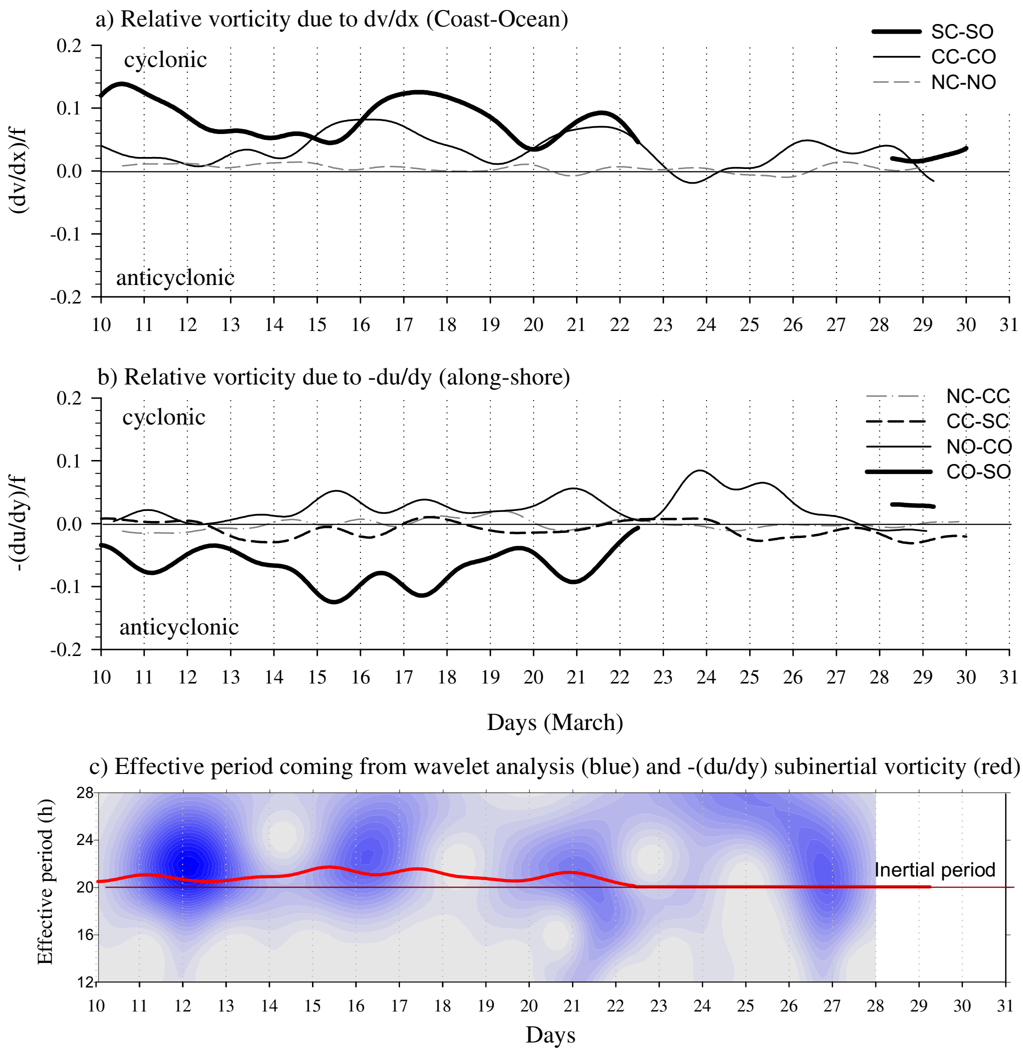

Fig. 8. (a) Relative vorticity of (dv/dx) and (b) $-(du/dy)$ subinertial currents; and (c) effective period coming from wavelet analysis of 10 m depth (Center-Ocean) and $-(du/dy)$ subinertial vorticity.

example, the ocean becomes resonant with the diurnal wind forcing, resulting in a large diurnal current response in the upper ocean.

4.2. Near-inertial variability: inertial–diurnal beating

The inner-shelf bursts of near-inertial currents occur every 3.5–4.5 days at the North-Coast site, are less frequent at the Center-Coast site, and do not appear to be related (Fig. 6a,b). On the other hand, the outer-shelf bursts of near-inertial currents vary between 4 and 6 days and show a stronger correspondence.

Cross-spectra between the surface near-inertial currents at all moorings and coastal winds (not shown) do not show significant coherence at diurnal or inertial frequencies, as in other studies (Rippeth et al., 2002).

Here we explore another possible explanation for the near-inertial intensifications related with a beat period between near-inertial currents and diurnal currents. According to Hyder et al. (2002), the beat period is $2\pi/(\omega - f)$, where ω is the diurnal frequency and f is the local inertial frequency. In the case of the North-Coast mooring at 10 m depth, the beat period is 128 h (5.3 days). However, this value does not correspond exactly with the intermittency observed in the NIOs at this mooring.

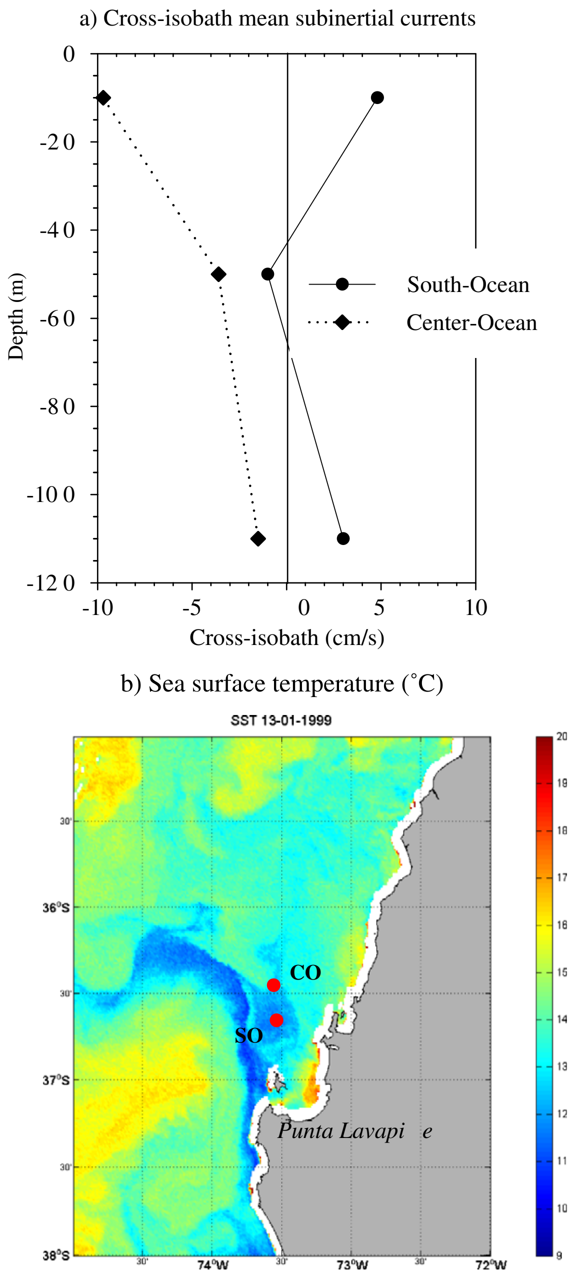

Fig. 9. (a) Cross-isobath mean current profiles from the South-Ocean (SO) and Center-Ocean (CO) moorings; (b) map of sea surface temperature (in °C) also showing mooring locations (red points).

To examine the beat period in more detail, Fig. 4a shows the spectrum of hourly raw data from 10 m depth at the North-Coast mooring. Near-inertial peaks appear at 20.58 and 19.88 h and diurnal peaks at 23.99 and 26.18 h. When we used 19.88 and 26.18 h to estimate the beat period, we obtained 3.4 days. This is closer to the period of near-inertial intensifications shown by the wavelet spectra of the hourly raw data (Fig. 4c). However, when we fit these two harmonics by a least-squares technique (satisfying the Rayleigh criterion for the separation of harmonic constituents) and removed their signal, we acquired a new spectrum without these frequencies (Fig. 4c) and a new wavelet spectrum in which near-inertial intensifications were now around 5 to 8 days (Fig. 4d). This agrees better than the beat period calculated using the other two constituents seen in Fig. 4a, namely, 20.58 and 23.99 h, which give around 6 days for a beating period.

The same argument can be used with the hourly raw data from 10 m depth at the Center-Coast mooring, where the near-inertial intensification was around 10–11 days. In this case, the major constituents were near-inertial (19.68, 20.20, 21.95 h) giving a beat period of around 10 days. Again, when we filtered these constituents, the near-inertial intensifications diminished nearly 8 days. These results are suggestive only; we have no evidence why specific near-inertial and diurnal periods should dominate the beating process, only that the certainly realistic combinations match the observed variability.

5. Conclusions

The observations presented here were collected on a wide and shallow continental shelf near one of the biologically most important coastal areas in the Chile–Peru upwelling system. During the field program in late summer (March 1994), 3–7 day events of upwelling-favorable south-westerly winds were accompanied by intense diurnal wind oscillations due to a sea breeze response. The principal conclusions are discussed below.

5.1. Offshore near-inertial current variability

Several authors have suggested that near-inertial wave intermittency may be related to the low-frequency horizontal and vertical shear (Kunze, 1985) and that the fluctuations in the along-shore flow can change the "effective" local Coriolis parameter ($f + \zeta/2$) by as much as 50% (Lerczak et al., 2001). In our case, the relative vorticity of the along-shore and cross-shore low-passed currents ranged from $0.1\,f$ to $-0.2\,f$ and there was an anticlockwise (positive) vorticity associated with the cross-shore flow near the shelf break. This anticlockwise vorticity may be related to cold water upwelled at Punta Lavapié that is then advected northward and frequently interacts with the shelf break off Concepción, forming fronts, filaments, or gyres.

Here we propose that offshore near-inertial events occur after upwelling-favorable winds (south-westerlies) when the diurnal wind is enhanced because the subtidal current response creates anticyclonic relative vorticity that shifts the effective Coriolis frequency lower, towards the diurnal frequency. As in Lerczak et al. (2001), the offshore ocean then is near resonant with the diurnal wind forcing.

5.2. Onshore near-inertial current variability

Near-inertial variability near the coast showed different patterns of intensifications (Fig. 6a,b,c). Bursts of near-inertial oscillations appeared each 3.5–4.5 days (North-Coast); 10–11 days (Center-Coast); and were not present at the South-Coast mooring, possibly due to the coastal boundary and friction. Changes in the effective Coriolis frequency were minor, suggesting weaker relative vorticity.

The argument of the beat period has been used by Van Haren et al. (2003) (f and the semidiurnal tidal lunar frequency) and by Rippeth et al. (2002) and Hyder et al. (2002) (f and diurnal currents), among others.

Here, we used different peaks of near-inertial and diurnal variability to show that bursts of near-inertial intensifications are sensitive to the peaks used to calculate the beat period. Although these peaks are not statistically significant, we propose that the coastal moorings exhibit a pattern of near-inertial variability that intensifies on time scales near the beat period as determined by the near-inertial and diurnal frequencies, ranging from 3–10 days. This analysis assumes the phasing of the near-inertial variability to be constant over the duration of the observations.

Sea breezes are known to produce near-inertial oscillations (Pollard, 1970; Pollard and Millard, 1970; Rippeth et al., 2002). In our case, south-westerly wind forcing between 0.1 and 0.4 Pa, at the diurnal frequency, associated with a summer sea breeze regime, is a candidate for driving the diurnal motions. On this diurnal temporal scale, diurnal and near-inertial currents produce bursts of near-inertial energy.

5.3. Near-inertial currents and coastal upwelling

Some of the biologically more productive areas located along the Chilean coast have been studied considering subinertial processes (such as coastal upwelling) and low-frequency effects on the coastal ecosystem (Sobarzo and Djurfeldt, 2004). However, this study shows that near-inertial oscillations may be another important process for this coastal ecosystem. This may be especially relevant for the coast off Concepción, where the near-inertial currents interact with a complex bathymetry (submarine canyons, wide shelf, shelf break) and with upwelling events (periods between 3 and 10 days). In this area, where tides are rather weak, near-inertial currents and upwelling may induce mixing in the water column but on different temporal and spatial scales. Whereas upwelling induces mixing near the coast and involves vertical currents, near-inertial currents influence the entire continental shelf with mixing that depends on the vertical shear intensity induced by horizontal currents. More studies will be required to determine the impact of the near-inertial oscillation on the mixing of the water column, especially near the upwelling front. Moreover, other studies along the Chilean coast and during other seasons of the year will be necessary to demonstrate the generality of the influence of the sea breeze on the near-inertial currents.

Acknowledgements

This work was carried out while one of the authors (M.S.) was a visiting scientist at the Woods Hole Oceanographic Institution, USA. This visit was sponsored by Fundación Andes (Chile) through a WHOI/University of Concepción Visiting Scientist Fellowship. Support from WHOI and Fundación Andes is acknowledged (D-13527). We want to thank Victor Ariel Gallardo, who provided the oceanographic data (CONICYT Project No. 1940998). Also, this research was partially supported by CONICYT (Chile) Grant No. 1040986. Support for S. Lentz was provided by the National Science Foundation, Grants OCE-0241292 and OCE-02820773.

References

Chen, C., Reid, R.O., Nowlin Jr., W.D., 1996. Near-inertial oscillations over Texas–Louisiana shelf. J. Phys. Oceanogr. 101 (C2), 3509–3524.

Federiuk, J., Allen, J.S., 1996. Model studies of near-inertial waves in flow over the Oregon continental shelf. J. Phys. Oceanogr. 26, 2053–2075.

Hill, E., Hickey, B., Shillington, F., Strub, T., Brink, K., Barton, E., Thomas, A., 1998. Eastern ocean boundaries coastal segment (E). In: The Sea, vol. 11. John Wiley & Sons Inc., pp. 30–67.

Hyder, P., Simpson, J.H., Christopoulos, S., 2002. Sea-breeze forced diurnal surface currents in the Thermaikos Gulf, North-west Aegean. Cont. Shelf Res. 22, 585–601.

Kunze, E.L., 1985. Near-inertial waves propagation in geostrophic shear. J. Phys. Oceanogr. 15, 544–565.

Lerczak, J.A., Hendershott, M.C., Winant, C.D., 2001. Observations and modelling of coastal internal waves driven by a diurnal sea breeze. J. Geophys. Res. 106 (C9), 19715–19729.

Millot, C., Crépon, M., 1981. Inertial oscillation on the continental shelf of the gulf of lions – observations and theory. J. Phys. Oceanogr. 11, 639–657.

Pawlowicz, R., Beardsley, B., Lentz, S., 2002. Classical tidal harmonic analysis including error estimates in MATLAB using T_TIDE. Comput. Geosci. 28, 929–937.

Pollard, R.T., 1970. On the generation by winds of inertial waves in the ocean. Deep-Sea Res. 17 (4), 795–812.

Pollard, R.T., Millard Jr., R.C., 1970. Comparison between observed and simulated wind-generated inertial oscillations. Deep-Sea Res. 17 (4), 813–821.

Rippeth, T.P., Simpson, J.H., Player, R.J., Garcia, M., 2002. Current oscillations in the diurnal–inertial band on the Catalonian shelf in spring. Cont. Shelf Res. 22, 247–265.

Rutllant, J., Garreaud, R., 1995. Meteorological air pollution potential for Santiago, Chile: towards an objective episode forecasting. Environ. Monitor. Assess. 34, 223–244.

Salat, J., Tintoré, J., Font, J., Dong-Ping, W., Vieira, M., 1992. Near-inertial motion on the shelf-slope front off north-east Spain. J. Geophys. Res. 97, 7277–7281.

Shaffer, G., Pizarro, O., Djurfeldt, L., Salinas, S., Rutllant, J., 1997. Circulation and low-frequency variability near the Chilean coast: remotely forced fluctuations during the 1991–92 El Niño. J. Phys. Oceanogr. 27, 217–235.

Shearman, R.K., 2005. Observations of near-inertial current variability on the New England shelf. J. Geophys. Res. 110, C02012. doi:10.1029/2004JC002341.

Simpson, J.E., 1995. Sea Breeze and Local Wind. Cambridge University Press.

Sobarzo, M., Djurfeldt, L., 2004. Coastal upwelling process on a continental shelf limited by submarine canyons, Concepción, central Chile. J. Geophys. Res. 109, C12012. doi:10.1029/2004JC002350.

Tintoré, J., Wang, D-P., García, E., Viúdez, A., 1995. Near-inertial motions in the coastal ocean. J. Mar. Syst. 6, 301–312.

Van Haren, H., Howarth, M.J., Jones, K., Ezzi, I., 2003. Autumnal reduction of stratification in the northern North Sea and its impact. Cont. Shelf Res. 23, 177–191.